THE UNIVERSITY *of* EDINBURGH

Edinburgh Research Explorer

Sparsity based Ground Moving Target Imaging via Multi-Channel SAR

Citation for published version:
Wu, D, Yaghoobi Vaighan, M & Davies, M 2015, Sparsity based Ground Moving Target Imaging via Multi-Channel SAR. in Sensor Signal Processing for Defence (SSPD). pp. 1-5.

Link:
Link to publication record in Edinburgh Research Explorer

Published In:
Sensor Signal Processing for Defence (SSPD)

OPEN ACCESS

Sparsity based Ground Moving Target Imaging via Multi-Channel SAR

Di Wu, Mehrdad Yaghoobi and Mike Davies

School of Engineering

University of Edinburgh

UK, EH9 3JL

Email: {D.Wu, m.yaghoobi-vaighan, mike.davies}@ed.ac.uk

Abstract—State-of-the-art Ground Moving Target Indicator (GMTI) schemes include the Displaced Phase Center Antenna (DPCA) and Along Track Interferometry (ATI) which are commonly used image-based dual-channel techniques for moving target detection. In the present paper, we provide a different perspective for solving GMTI tasks by generalising the ground moving targets imaging as an parameter estimation and optimisation problem. A sparsity based ground target imaging approach is described to improve the image quality for moving targets and estimate their states. By exploiting the fact that moving targets are highly sparse in the observed scene and feasible velocity space, the proposed method constructs a velocity map for the illuminated region, and combines this map with a sparsity based optimisation algorithm to realise the image formation. The performance of the presented method is demonstrated through GOTCHA airborne SAR data set.

Index Terms—SAR, GMTI, sparsity, compressed sensing, velocity map

I. INTRODUCTION

One of the basic principles of SAR is to assume a stationary scene. Therefore moving targets will induce displacement and blurring in the image. Ground Moving Target Indicator (GMTI) aims to detect the moving targets in the SAR image and estimate their velocities which are of great value for the battlefield awareness and information gathering. The entire SAR/GMTI systems often consist of several signal processing steps such as pre-processing, range compression, clutter cancellation, target detection, geo-location, motion parameters estimation and SAR image formation [1][2][3].

Displaced Phase Center Antenna (DPCA), Along Track Interferometry (ATI) and Space-time Adaptive Processing (STAP) are the multi-channel methods which have been widely used in the SAR community. DPCA and ATI [4][5] attempt to expose the moving targets from the SAR images of different channels with magnitudes and interference phases respectively. However the target radial velocities can be derived from the ATI results directly and DPCA is not capable of doing that. STAP [6] is well known to be computationally expensive, and it is hampered by the false alarm rates especially in non-homogeneous urban environments. Also in 2012, Prunte proposed to indicate moving targets based on multi-channel SAR using compressed sensing [7]. The proposed method is utilising the sparsities pixel-wise in the image domain.

In this paper, we present a model to link up certain parts of the processing chain in multi-channel SAR/GMTI and represent them as a generalised optimisation problem. By introducing the sparsities in the proposed model, i.e. the number of moving targets is reasonably small compared to the size of the observed scene, ground moving targets can be mapped and their motion parameters can be estimated. We hope this novel model can provide an alternative perspective for viewing SAR/GMTI problems.

The remainder of this paper is organized as follows. Section two describes the signal model in a typical dual-channel SAR system. In section three, the sparsity based moving target imaging model is presented. We first discuss the channel balancing techniques to co-register different channels. Then we present the mechanism of traditional SAR imaging and clutter cancellation algorithms, and finally introduce the sparse regularized optimisation model to realise simultaneous SAR/GMTI. In section four, the real airborne SAR data is utilised to demonstrate the performances of the proposed model. Conclusions and future work are presented in section five.

II. SIGNAL MODELING

The proposed framework is presently demonstrated through a typical dual-channel SAR system in this paper, but it can be generalised to the scenarios with more than two channels. The geometry with a moving target in the observed scene is shown in Fig. 1. The phase centres of the fore-antenna and aft-antenna are spatially separated by a distance d on the flight path of the platform. The Cartesian velocity components of the moving target are denoted as $(v^{(x)}, v^{(y)}, v^{(z)})$ which can be converted to $(v^{(az)}, v^{(r)})$ in the azimuth and radial directions. Let the azimuth time of the transmitted pulses be τ_n where $n = \{1, 2, ..., N\}$ is the pulse number. Then $\mathbf{r}(\tau_n)$ is the position of the target at τ_n, $r_i^{(t)}(\tau_n)$ and $r_i^{(o)}(\tau_n)$ represent the distances from the moving target to the $i-th$ antenna and the distance from the scene origin to the corresponding antenna position. Also the platform velocity within a short sub-aperture is approximated by a constant v_p, and f_{PRF} is the pulse repetition frequency (PRF).

In the remainder of the paper, we apply the stop-and-hop approximation which assumes that the targets and platform have constant positions during the RF propagation of one pulse unless otherwise stated. After the de-chirping process, in which the platform motion has been compensated with
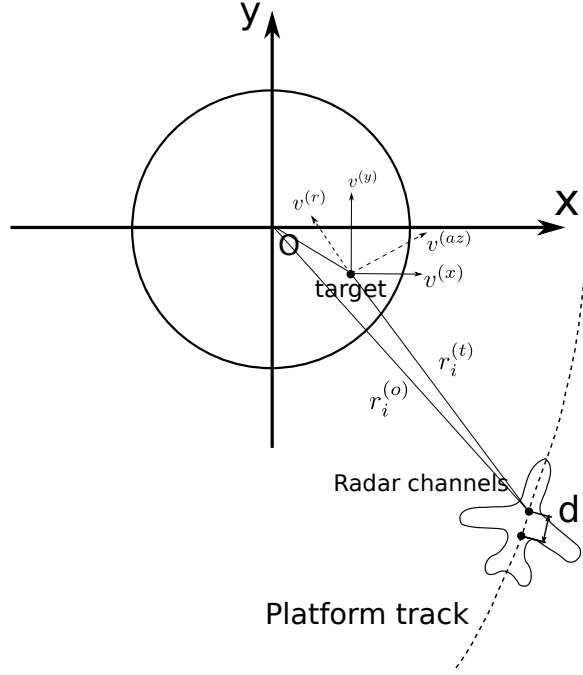
Fig. 1. The geometry of a dual-channel SAR system with a moving target in the observed scene.

reference to the scene origin, the channel 1 (fore-antenna) and 2 (aft-antenna) discrete received signals of a single moving target located at $\mathbf{r}(\tau_n)$ are:

$$Y_i(f_k, \tau_n) = A_i \sigma(\mathbf{r}(\tau_n)) \exp\left(-\frac{j4\pi f_k u_i(\tau_n)}{c}\right) \quad (1)$$

where $\{f_k | k = 1, 2, ..., K\}$ denotes the range frequencies; A_i is the nominal factor of the received signal for the $i-th$ channel which accounts for the beam pattern and energy loss; $\sigma(\mathbf{r}(\tau_n))$ is the complex reflectivity of this moving target; c represents the speed of light and $u_i(\tau_n)$ denotes the differential range $r_i^{(t)}(\tau_n) - r_i^{(o)}(\tau_n)$.

We assume that the moving target has constant velocity during the sub-aperture time, then the instantaneous spatial location of the target $\mathbf{r}(\tau_n)$ can be expressed as $(x_0 + \tau_n v^{(x)}, y_0 + \tau_n v^{(y)}, z_0 + \tau_n v^{(z)})$ where (x_0, y_0, z_0) stands for the initial position of the target. The goal of SAR/GMTI is to estimate the target states including the geolocation $\mathbf{r}(\tau_n)$ and velocities $(v^{(x)}, v^{(y)}, v^{(z)})$ given the received signals $Y_1(f_k, \tau_n)$ and $Y_2(f_k, \tau_n)$.

III. SPARSITY BASED MOVING TARGET IMAGING

Based on the dual-channel SAR system we describe the proposed sparsity based moving target imaging approach and its relationship with commonly used SAR/GMTI techniques.

A. Pre-processing and Channel Balancing

For subtractive GMTI methods such as ATI and DPCA, the differences between channels are exploited to detect targets and suppress the clutter. Thus it is crucial to equalise the channel transfer functions in the pre-processing step. With

channel balancing techniques, we attempt to retrieve the same responses for stationary targets between different channels.

Since the baseline d in the SAR system is along the platform track, the received echo of the aft-antenna can be viewed as the delayed received signal of the fore-antenna if the observed region does not change over time. We can illustratively assume that $\mathbf{r}_1^{(c)}(\tau_n) = \mathbf{r}_2^{(c)}(\tau_n + \Delta)$ where $\mathbf{r}_i^{(c)}(\tau_n)$ denotes the location of the $i-th$ antenna at τ_n and $\Delta = d/v_p$ represents the delay between two channels. Here $\tau_n + \Delta$ may not correspond to an exact pulse time. Then the differential range $u_2(\tau_n + \Delta)$ can be rewritten as

$$
\begin{aligned}
u_2(\tau_n + \Delta) &= r_2^{(t)}(\tau_n + \Delta) - r_2^{(o)}(\tau_n + \Delta) \\
&= \|\mathbf{r}_2^{(c)}(\tau_n + \Delta) - \mathbf{r}(\tau_n + \Delta)\| - \|\mathbf{r}_2^{(c)}(\tau_n + \Delta)\| \\
&= \|\mathbf{r}_1^{(c)}(\tau_n) - \mathbf{r}(\tau_n + \Delta)\| - \|\mathbf{r}_1^{(c)}(\tau_n)\| \quad (2)
\end{aligned}
$$

If the targets are isotropic and their reflectivities keep the same over time then we can derive from (1) that

$$
\begin{aligned}
Y_1(f_k, \tau_n) = A_1 \sigma(\mathbf{r}(\tau_n)) \times \\
\exp\left(-\frac{j4\pi f_k(\|\mathbf{r}_1^{(c)}(\tau_n) - \mathbf{r}(\tau_n)\| - \|\mathbf{r}_1^{(c)}(\tau_n)\|)}{c}\right)
\end{aligned}
$$
(3)

$$
\begin{aligned}
Y_2(f_k, \tau_n + \Delta) = A_2 \sigma(\mathbf{r}(\tau_n)) \times \\
\exp\left(-\frac{j4\pi f_k(\|\mathbf{r}_1^{(c)}(\tau_n) - \mathbf{r}(\tau_n + \Delta)\| - \|\mathbf{r}_1^{(c)}(\tau_n)\|)}{c}\right)
\end{aligned}
$$
(4)

where $Y_2(f_k, \tau_n + \Delta)$ is the time-shifted version of $Y_2(f_k, \tau_n)$ which can be estimated by the multiplication in the frequency domain with a Δ-induced phase shift term. We denote this as $\widetilde{Y}_2(f_k, \tau_n) = Y_2(f_k, \tau_n + \Delta)$.

It can be seen that the velocity and position information of the moving targets are fully described by the last exponential terms in (3) and (4). We also need to balance the channels to equalise A_1 and A_2 as done for example in [8]. In this way, $Y_1(f_k, \tau_n)$ and $\widetilde{Y}_2(f_k, \tau_n)$ are supposed to be the same for stationary targets. We will employ this channel balancing technique to pre-process the SAR data in the remainder of the paper.

B. SAR Imaging and Clutter Cancelation

Numerous algorithms have been proposed for SAR image formation by investigating the trade-off between complexity and image quality. For simplicity we will focus on matched filter based techniques.

Let the discrete grid on which the image is formed be $\mathbb{G}_{ml} = (x_m, y_l, 0)$ and $d_{mln} = \|\mathbf{r}_1^{(c)}(\tau_n) - \mathbb{G}_{ml}\| - \|\mathbf{r}_1^{(c)}(\tau_n)\|$, where $m = \{1, 2, ..., M\}$ and $l = \{1, 2, ..., L\}$. Then the observed scene can be viewed as the collection of the targets in this grid. Here the elevation is assumed to be zero for the convenience of subsequent analysis. The formed

SAR images with the matched filter method are

$$X_1(m,l) = \sum_{k=1}^{K} \sum_{n=1}^{N} Y_1(f_k, \tau_n) \exp\left(\frac{j4\pi f_k d_{mln}}{c}\right) \quad (5)$$

$$X_2(m,l) = \sum_{k=1}^{K} \sum_{n=1}^{N} \widetilde{Y}_2(f_k, \tau_n) \exp\left(\frac{j4\pi f_k d_{mln}}{c}\right) \quad (6)$$

Typical clutter suppression methods such as DPCA and ATI exploit the differences between (5) and (6) to reveal the moving targets. Specifically, DPCA is achieved by subtracting (6) from (5), and ATI is realised by multiplying (5) with the conjugate of (6). For DPCA, we have that

$$X_1(m,l) - X_2(m,l)$$
$$= \sum_{k=1}^{K} \sum_{n=1}^{N} Y_1(f_k, \tau_n) \exp\left(\frac{j4\pi f_k d_{mln}}{c}\right)\left(1 - \exp\left(-\frac{j4\pi f_k(w_{mln})}{c}\right)\right) \quad (7)$$

where $w_{mln} = \|\mathbf{r}_1^{(c)}(\tau_n) - \mathbf{r}_{ml}(\tau_n + \Delta)\| - \|\mathbf{r}_1^{(c)}(\tau_n) - \mathbf{r}_{ml}(\tau_n)\|$. At azimuth time τ_n, the position of the target which was initially located at $(x_m, y_l, 0)$ is denoted as $\mathbf{r}_{ml}(\tau_n)$. w_{mln} can then be approximated by $v_{ml}^{(r)}\Delta$ where $v_{ml}^{(r)}$ is the radial velocity of this target. Also $\exp(-j4\pi f_k w_{mln}/c)$ can be approximated with a constant if the target remains in the same range resolution cell during the time interval Δ [9]. Then equation (7) can be rewritten as:

$$X_1(m,l) - X_2(m,l) \approx X_1(m,l)\left(1 - \exp\left(-\frac{j4\pi f_0(v_{ml}^{(r)}\Delta)}{c}\right)\right) \quad (8)$$

where f_0 is denoted as the centre frequency of the transmitted signal chirps. Similarly for ATI we have that

$$X_1(m,l) \times X_2^*(m,l) \approx |X_1(m,l)|^2 \exp\left(\frac{j4\pi f_0(v_{ml}^{(r)}\Delta)}{c}\right) \quad (9)$$

It can be seen that (8) and the phase of (9) are zero for stationary targets ($v_{ml}^{(r)} = 0$). Particularly the DPCA results are approximately the velocity-scaled reflectivities of the moving targets. Hence, clutter suppression techniques such as DPCA and ATI enable us to project out stationary targets. Also the radial velocities $\{v_{ml}^{(r)} | m = 1, 2, ..., M; l = 1, 2, ..., L\}$ can be estimated directly based on the phase of (9).

C. Sparse Regularized SAR/GMTI

There has been a number of SAR imaging algorithms with super-resolution effects by utilising the image sparsity [10][11]. The proposed approaches can mitigate the sidelobes in SAR images and reconstruct the bright image elements. In GMTI applications the whole observed scene is not sparse but the moving targets are often sparse. In this way, if we can build up the linear projection from the raw data to the moving targets and its inverse projection, the techniques which are commonly used in compressed sensing [12] can then be leveraged to form the image of these sparse targets.

Let $\mathbf{X}_i = \{X_i(m,l)\} \in \mathbb{C}^{M \times L}$ be the SAR image of the $i - th$ channel; $\mathbf{Y}_1 = \{Y_1(f_k, \tau_n)\} \in \mathbb{C}^{K \times N}$ and $\widetilde{\mathbf{Y}}_2 = \widetilde{Y}_2(f_k, \tau_n) \in \mathbb{C}^{K \times N}$ be the received phase history of the 1st channel and the balanced phase history of the 2nd channel respectively. Based on (1) we can write the signal model in matrix-vector form as $\mathbf{Y}_1 = \Phi_F(\mathbf{X}_1)$ where Φ_F is the forward projection operator.

Note that DPCA is essentially the linear projection from $\mathbf{Y}_1 - \widetilde{\mathbf{Y}}_2$ to $\mathbf{X}_1 - \mathbf{X}_2$, thereby all stationary scatterers are removed. Therefore a simple sparsity based GMTI could exploit the following optimisation problem:

$$\min_{\mathbf{X}} \|\mathbf{Y}_1 - \widetilde{\mathbf{Y}}_2 - \Phi_F(\mathbf{X})\|_F^2 + \lambda\|\mathbf{X}\|_1$$
$$s.t. \quad \mathbf{X} \in \mathbb{C}^{M \times L} \quad (10)$$

where $\|\|_F$ represents the Frobenius norm, λ is a positive tuning parameter, and $\mathbf{X}$ is the sparsified image of moving targets and sparsity in $\mathbf{X}$ is encouraged through the inclusion of the L_1 norm penalty function. Note that this formulation still takes no account of the velocity effect at this stage, and the moving targets will be displaced and blurred in the resulting $\mathbf{X}$.

A more advanced sparsity based SAR/GMTI formulation can also be derived that simultaneously takes into account the sparsity of the moving targets and estimates their velocities. Let $\mathbf{V} = (\mathbf{V}^{(x)}, \mathbf{V}^{(y)}, 0)$ denote the velocity maps for a specific observed scene $\mathbf{X}$ (here $\mathbf{X}$ includes stationary and moving targets) where $\mathbf{V}^{(x)} = \{v_{ml}^{(x)}\} \in \mathbb{R}^{M \times L}$ and $\mathbf{V}^{(y)} = \{v_{ml}^{(y)}\} \in \mathbb{R}^{M \times L}$ are the velocity components of $\mathbb{G}_{ml}$ in x and y directions. The velocity map $\mathbf{V}$ can be interpreted as granting each image element with specific velocity components. With reference to the geometry Fig. 1, the velocity map can be directly converted to the corresponding azimuth velocity $\mathbf{V}^{(az)} = \{v_{ml}^{(az)}\} \in \mathbb{R}^{M \times L}$ and radial velocity $\mathbf{V}^{(r)} = \{v_{ml}^{(r)}\} \in \mathbb{R}^{M \times L}$.

In this model we make the reasonable assumption that there is only one dominant velocity for each image element. This assumption makes the reconstructions for a specific physical position (m,l) to be 1-sparse along the $\mathbf{V}$ axis. Incorporating the velocities into the signal model it can be shown that:

$$Y_1(f_k, \tau_n) = \sum_{m=1}^{M} \sum_{l=1}^{L} X(m,l) \exp\left(-\frac{j4\pi f_k d'_{1mln}}{c}\right) \quad (11)$$

$$\widetilde{Y}_2(f_k, \tau_n)$$
$$= \sum_{m=1}^{M} \sum_{l=1}^{L} X(m,l) \exp\left(-\frac{j4\pi f_k d'_{1mln}}{c}\right) \exp\left(-\frac{j4\pi f_k v_{ml}^{(r)}\Delta}{c}\right) \quad (12)$$

where $d'_{1mln} = \|\mathbf{r}_1^{(c)}(\tau_n) - \mathbb{G}_{ml} - (\tau_n v_{ml}^{(x)}, \tau_n v_{ml}^{(y)}, 0)\| - \|\mathbf{r}_1^{(c)}(\tau_n)\|$.

Given a velocity map $\mathbf{V}$, we can denote the projection operator from the physical space $\mathbf{X}$ to the phase history $\mathbf{Y}_1$ and $\widetilde{\mathbf{Y}}_2$ as $\Phi_F^{\mathbf{V}}$ and $\widetilde{\Phi}_F^{\mathbf{V}}$ respectively. The following model is hereby

introduced to simultaneously estimate the target's states and form the SAR images:

$$\min_{\mathbf{X},\mathbf{V}}\|\mathbf{Y}_1-\Phi_F^{\mathbf{V}}(\mathbf{X})\|_F^2+\|\widetilde{\mathbf{Y}}_2-\widetilde{\Phi}_F^{\mathbf{V}}(\mathbf{X})\|_F^2+\lambda\|\mathbf{V}^{(x)}\|_0+\lambda\|\mathbf{V}^{(y)}\|_0$$

$$s.t. \quad \mathbf{X}\in\mathbb{C}^{M\times L},\mathbf{V}^{(x)}\in\mathbb{R}^{M\times L},\mathbf{V}^{(y)}\in\mathbb{R}^{M\times L}$$

$$\mathrm{supp}(\mathbf{V}^{(x)})=\mathrm{supp}(\mathbf{V}^{(y)})$$

(13)

where λ is a positive tuning parameter. The resulting $\mathbf{X}$ represents the reflectivities of the observed scene including both stationary and moving targets. Practically solving (13) is challenging and therefore in the next section we will explore a solution based on a partial formulation of (13) that further leverages the ATI technique.

IV. Processing Results of the GOTCHA Data

The sparsity method is demonstrated through the AFRL GOTCHA data set [13]. The described scope contains an X-band SAR system with three phase centers and a number of moving vehicles in an urban environment. The ground truth data of one vehicle is provided. To be specific, the transmitted chirp is centred at 9.6 GHz, the phase history is collected over 71 seconds interval, and the PRF is 2.17 kHz. Furthermore, as presented in [13], the data was range-gated from 5400 range samples to 384 sub bins to decrease the required storage. The scenario can be found in Fig. 2. Based on the ground truth data, the target trajectory is illustrated by the red path. With reference to the streets and roads, the target trajectory is displaced along the x direction for about 20 meters. These displacements result from the elevation variations of the observed terrain. In this section, we consider the data from first two channels at the $46-th$ second snapshot of the scenario with 200 pulses (about 0.1 second interval) around.
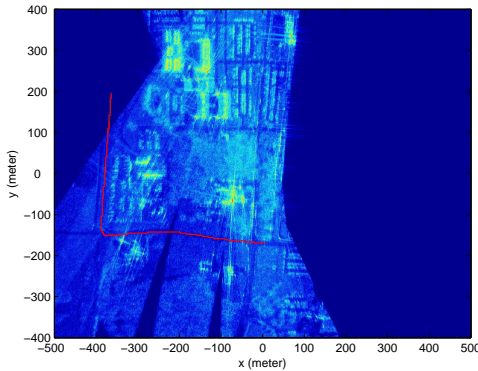

Fig. 2. The reconstructed SAR image in dB with partial data to show the GMTI scenario. Here we assume a flat terrain and the accelerated version of (5) is employed. The red path stands for the target trajectory based on the ground truth data.

To preprocess the data, we first run the inverse operation of the the range gating and replace the unknown range gates with zero. The phase histories are reorganized into data matrices $\mathbf{Y}_1\in\mathbb{C}^{5400\times 200}$ and $\mathbf{Y}_2\in\mathbb{C}^{5400\times 200}$. We then apply the 2D channel balancing technique [8] to the first two channels and the calibrated phase histories are $\mathbf{Y}_1$ and $\widetilde{\mathbf{Y}}_2$. To decrease the computational complexity, here we approximately crop the phased history in the 2D Fourier transform domain with rectangular windows (49 points in range and 10 points in azimuth directions) to focus on the known target. The cropped phase histories are denoted as $\mathbf{Y}_1^{(t)}\in\mathbb{C}^{5400\times 200}$ and $\widetilde{\mathbf{Y}}_2^{(t)}\in\mathbb{C}^{5400\times 200}$. The formed image of $\mathbf{Y}_1^{(t)}$ with (5) can be found in Fig. 3.
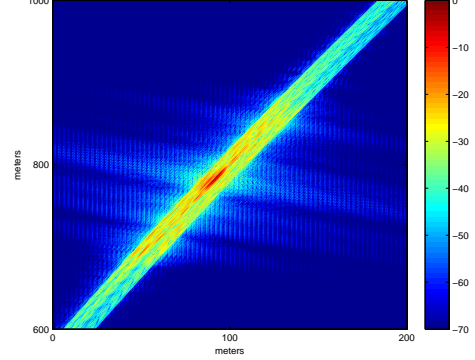

Fig. 3. The corresponding SAR image of the cropped phase history. The image is displayed in -70∼0 dB. No velocity is assumed in this image. The target appears to be displaced and blurred.

It is well known that the radial velocities can be estimated from the phase information using ATI. Therefore, to simplify the problem, based on ATI, we still estimate the radial velocity $\mathbf{V}^{(r)}$ by $c\Theta/(4\pi f_0\Delta)$ given that the phases of the ATI results are Θ. Here the baseline $d=0.238m$ can be estimated in the preprocessing [2] and the radial velocity is chosen to be the mean value of nonzero $\mathbf{V}^{(r)}$. Once we have $\mathbf{V}^{(r)}$, it is straight forward to map $\mathbf{V}^{(r)}$ and $\mathbf{V}^{(az)}$ to $\mathbf{V}$ based on the geometry, and we denote this as $\mathbf{V}=\Upsilon(\mathbf{V}^{(az)},\mathbf{V}^{(r)})$. We now have the following model:

$$\min_{\mathbf{X},\mathbf{V}^{(az)}}\|\mathbf{Y}_1^{(t)}-\widetilde{\mathbf{Y}}_2^{(t)}-\Phi_F^{\mathbf{V}}(\mathbf{X})\|_F^2+\lambda\|\mathbf{X}\|_1$$

$$s.t.\quad \mathbf{X}\in\mathbb{C}^{M\times L},\mathbf{V}^{(az)}\in\mathbb{R}^{M\times L},\mathbf{V}=\Upsilon(\mathbf{V}^{(az)},\mathbf{V}^{(r)})$$

$$\mathrm{supp}(\mathbf{X})=\mathrm{supp}(\mathbf{V}^{(az)})$$

(14)

As $\mathbf{Y}_1^{(t)}$ and $\widetilde{\mathbf{Y}}_2^{(t)}$ are focusing on the target, the elements in $\mathbf{V}^{(az)}$ can be assigned to a single $v^{(az)}$ throughout the image. Here a naive method to solve (14) is implemented. We first compute (14) using five iteration FISTA algorithm [14] ($\lambda=0.3\cdot 2\|\Phi_F^{\mathbf{V}H}(\mathbf{Y}_1^{(t)}-\widetilde{\mathbf{Y}}_2^{(t)})\|_\infty$) with different $v^{(az)}$ independently. The objective value of (14) with each specific $v^{(az)}$ is recorded. The optimal $v^{(az)}$ and $\mathbf{X}$ are chosen to correspond with the minimised objective value. The objective value against $v^{(az)}$ plot is shown in Fig. 4. The estimated $\mathbf{X}$ gives the relocated and refocused image of the moving target which is shown in Fig. 5.
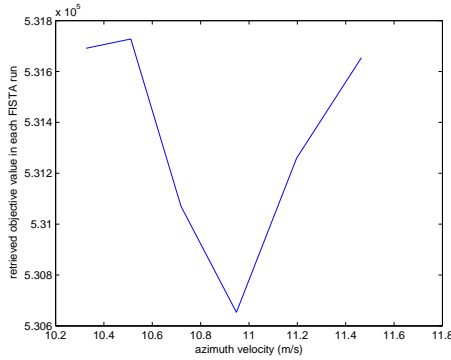
Fig. 4. Resulting objective values with respect to different $v^{(az)}$ based on the FISTA for (14).
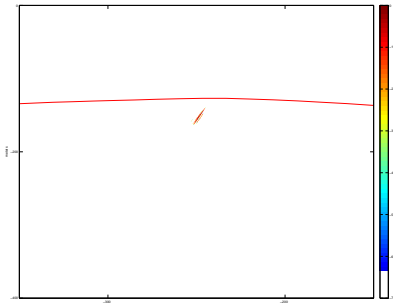

Fig. 5. The reconstructed image in dB of the moving target. Five iteration FISTA is employed for the $46 - th$ second with 200 pulses. The red line indicates the ground truth data.

TABLE I
COMPARISONS BETWEEN THE GROUND TRUTH AND ESTIMATIONS

	Ground Truth	Estimations
x (m)	-220.1	-249
y (m)	-127.9	-152
z (m)	-3.2	0
range distance (m)	1.038e4	1.039e4
$v^{(r)}$ (m/s)	-9.45	-9.77
$v^{(az)}$ (m/s)	9.64	10.95
overall v (m/s)	13.5	14.67

The estimation results are concluded in Table I. It can been seen from Fig. 2 that the ground truth trajectory has about 20 meters deviation in x direction due to the terrain elevation. The estimated target position is also shifted towards the negative x direction in the image, and the range distance ground truth coincides with the estimation result. Note that all the estimations are based on a very short sub-aperture, a larger sub-aperture is likely to increase the accuracy as long as the constant velocity assumptions still hold.

V. CONCLUSION

This paper presents a sparse regularized model for multi-channel SAR/GMTI. Specifically we show how the SAR/GMTI task can be generalised as an optimisation problem and how the sparsity can be used to help estimate the estimate targets' state and form SAR images. The experimental results based on real GOTCHA GMTI data illustrate the effectiveness of the proposed model. In practice, SAR/GMTI is likely to encounter the problems such as the imperfections in channel balancing, the ambiguities in velocity estimations and the demand on computational power. These will be investigated in the future work.

REFERENCES

[1] R. Deming, M. Best, and S. Farrell, "Simultaneous SAR and GMTI using ATI/DPCA," *Proc. SPIE*, vol. 9093, pp. 90 930U–90 930U–19, 2014.

[2] B. Guo, D. Vu, L. Xu, M. Xue, and J. Li, "Ground moving target indication via multichannel airborne SAR," *IEEE T. Geoscience and Remote Sensing*, vol. 49, no. 10, pp. 3753–3764, 2011.

[3] J. Yang, C. Liu, and Y. Wang, "Detection and imaging of ground moving targets with real SAR data," *IEEE T. Geoscience and Remote Sensing*, vol. 53, no. 2, pp. 920–932, 2015.

[4] S. Chiu and C. Livingstone, "A comparison of displaced phase centre antenna and along-track interferometry techniques for RADARSAT-2 ground moving target indication," *Canadian Journal of Remote Sensing*, vol. 31, no. 1, pp. 37–51, 2005.

[5] I. Sikaneta and C. Gierull, "Ground moving target detection for along-track interferometric SAR data," in *Aerospace Conference, 2004. Proceedings. 2004 IEEE*, vol. 4, March 2004, pp. 2227–2235 Vol.4.

[6] J. Ward, "Space-time adaptive processing for airborne radar," in *Space-Time Adaptive Processing (Ref. No. 1998/241), IEE Colloquium on*, Apr 1998, pp. 2/1–2/6.

[7] L. Prunte, "GMTI from multichannel SAR images using compressed sensing," in *Synthetic Aperture Radar, 2012. EUSAR. 9th European Conference on*, April 2012, pp. 199–202.

[8] C. Gierull, "Digital channel balancing of along-track interferometric SAR data," in *Technical Memorandum DRDC Ottawa TM 2003-024*. Defence R&D, Ottawa, Canada, March 2003.

[9] R. W. Deming, "Along-track interferometry for simultaneous SAR and GMTI: application to gotcha challenge data," *Proc. SPIE*, vol. 8051, pp. 80 510P–80 510P–18, 2011.

[10] S. Kelly and M. Davies, "RFI suppression and sparse image formation for UWB SAR," in *Radar Symposium (IRS), 2013 14th International*, vol. 2, June 2013, pp. 655–660.

[11] M. Cetin and R. L. Moses, "SAR imaging from partial-aperture data with frequency-band omissions," *Proc. SPIE*, vol. 5808, pp. 32–43, 2005.

[12] M. Fornasier and H. Rauhut, "Compressive sensing," in *Handbook of Mathematical Methods in Imaging*. Springer, 2011, pp. 187–228.

[13] S. M. Scarborough, C. H. Casteel, Jr., L. Gorham, M. J. Minardi, U. K. Majumder, M. G. Judge, E. Zelnio, M. Bryant, H. Nichols, and D. Page, "A challenge problem for SAR-based GMTI in urban environments," *Proc. SPIE*, vol. 7337, pp. 73 370G–73 370G–10, 2009.

[14] A. Beck and M. Teboulle, "A Fast Iterative Shrinkage-Thresholding Algorithm for Linear Inverse Problems," *SIAM Journal on Imaging Sciences*, vol. 2, no. 1, pp. 183–202, Mar. 2009.